Observation of relativistic electron microbursts in conjunction with intense radiation belt whistler-mode waves

K. Kersten,[1] C. A. Cattell,[1] A. Breneman,[1] K. Goetz,[1] P. J. Kellogg,[1] J. R. Wygant,[1] L. B. Wilson III,[2] J. B. Blake,[3] M. D. Looper,[3] and I. Roth[4]

Received 18 January 2011; revised 14 March 2011; accepted 28 March 2011; published 28 April 2011.

[1] We present multi-satellite observations of large amplitude radiation belt whistler-mode waves and relativistic electron precipitation. On separate occasions during the Wind petal orbits and STEREO phasing orbits, Wind and STEREO recorded intense whistler-mode waves in the outer nightside equatorial radiation belt with peak-to-peak amplitudes exceeding 300 mV/m. During these intervals of intense wave activity, SAMPEX recorded relativistic electron microbursts in near magnetic conjunction with Wind and STEREO. This evidence of microburst precipitation occurring at the same time and at nearly the same magnetic local time and *L*-shell with a bursty temporal structure similar to that of the observed large amplitude wave packets suggests a causal connection between the two phenomena. Simulation studies corroborate this idea, showing that nonlinear wave–particle interactions may result in rapid energization and scattering on timescales comparable to those of the impulsive relativistic electron precipitation. **Citation:** Kersten, K., C. A. Cattell, A. Breneman, K. Goetz, P. J. Kellogg, J. R. Wygant, L. B. Wilson III, J. B. Blake, M. D. Looper, and I. Roth (2011), Observation of relativistic electron microbursts in conjunction with intense radiation belt whistler-mode waves, *Geophys. Res. Lett.*, *38*, L08107, doi:10.1029/2011GL046810.

1. Introduction

[2] Whistler-mode waves have seen a resurgence as a potential energization and loss mechanism for radiation belt electrons following the discovery by *Cattell et al.* [2008] of whistler-mode waves with amplitudes orders of magnitude larger than previously observed. Past studies have employed spectral analysis in the characterization of whistler chorus [e.g., *Burtis and Helliwell*, 1976; *Santolík et al.*, 2003, and references therein]. While these studies have established a picture of the spatial occurrence and characteristic frequencies of the whistler chorus, the use of time–averaged spectral analysis has drastically underestimated the range of wave amplitudes. Recent observations of large amplitude whistler-mode waves highlight the need for a closer look at individual wave packet structure and the potential for rapid energization and scattering of radiation belt electrons through nonlinear wave–particle interactions [*Cattell et al.*, 2008; *Cully et al.*, 2008; P. J. Kellogg et al., Large amplitude whistlers in the magnetosphere observed with Wind–WAVES, submitted to *Journal of Geophysical Research*, 2010].

[3] Microbursts – bursty energetic particle precipitation to the ionosphere – are one of the most telling and commonly observed signs of the rapid scattering of radiation belt electrons. It is believed that low energy microbursts are closely tied to whistler chorus enhancements [e.g., *Oliven and Gurnett*, 1968; *Oliven et al.*, 1968]; the connection between relativistic (>1 MeV) electron microbursts and chorus is not as established. Relativistic electron microbursts (REMB) were first reported by *Imhof et al.* [1992], and initial observations showed no correspondence to the whistler chorus. *Blake et al.* [1996] cataloged the occurrence of relativistic electron microbursts to find spatially localized regions of impulsive precipitation bursts, suggesting the phenomenon is a result of rapid scattering processes rather than a breakdown in the adiabatic motion of trapped particles. Using Polar and SAMPEX data, *Lorentzen et al.* [2001] reported REMB at all local times with peak occurrence from 0200 to 1000 MLT. Prompted by spectral evidence of correlated dispersive chorus elements in the Polar swept frequency receiver and high-frequency waveform receiver, they suggested that coherent, oblique whistler chorus elements may provide the scattering mechanism that drives the observed precipitation.

[4] The occurrence of microbursts in conjunction with coherent, oblique large amplitude whistler wave packets was first reported by *Cattell et al.* [2008] using the STEREO-B and SAMPEX satellites. The observed large amplitude whistler-mode waves exhibit properties not typically associated with the whistler chorus, e.g., their very large amplitudes, oblique propagation, and non-dispersive monochromatic signature. Recent examination of Wind data reveals the common occurrence of similar large amplitude radiation belt whistler-mode waves (Kellogg et al., submitted manuscript, 2010). We show STEREO/SAMPEX and Wind/SAMPEX observations of microbursts in conjunction with very large amplitude whistler-mode waves. The microburst precipitation exhibits a temporal structure similar to that of the observed large amplitude whistler wave packets. Test particle simulations show that the bursty large amplitude waves may accelerate electrons to MeV energies while at the same time scattering them into the loss cone [*Cattell et al.*, 2008; *Bortnik et al.*, 2008]. These results suggest that very large amplitude radiation belt whistler wave

[1]School of Physics and Astronomy, University of Minnesota, Twin Cities, Minneapolis, Minnesota, USA.
[2]NASA Goddard Space Flight Center, Greenbelt, Maryland, USA.
[3]Space Science Department, The Aerospace Corporation, El Segundo, California, USA.
[4]Space Sciences Laboratory, University of California, Berkeley, California, USA.

Copyright 2011 by the American Geophysical Union.
0094-8276/11/2011GL046810

packets may drive subsecond enhancements in relativistic electron precipitation.

2. Satellites and Instrumentation

[5] The Wind satellite, launched in 1994, entered highly inclined petal orbits in late 1998 and early 2000 beginning with nightside traversals of the equatorial radiation belts. Wind carries a suite of instruments designed to make high time resolution measurements of AC electromagnetic fields [*Bougeret et al.*, 1995]. Using two orthogonal spin plane dipole probes (E_x, 100 m tip-to-tip; E_y, 15 m tip-to-tip) and a spin axis dipole (E_z, 12 m tip-to-tip), the WAVES Fast Time Domain Sampler (TDSF) records two-component AC-coupled electric fields at sampling rates up to 125 kS/s. The TDS instrument samples continuously, buffering 2048-point samples categorized by the peak amplitude detected. Due to limited onboard memory and telemetry bandwidth, only the largest amplitude captures are saved and transmitted to ground. While this configuration does not provide continuous coverage, the 7.5 kS/s (duration 273 ms) TDSF events used in this study constitute a survey of the most intense wave activity.

[6] The twin STEREO satellites were launched in 2006 into phasing orbits providing four passes through the nightside radiation belts [*Driesman et al.*, 2008]. The final phasing orbit brought the two spacecraft to perigee at $L \simeq 2$ at roughly 2100 MLT from which they emerged through the pre-dawn equatorial radiation belts. The three-axis stabilized STEREO spacecraft employ three mutually orthogonal 6 m stacer antennas coupled to a TDS capable of sampling at up to 250 kS/s [*Bougeret et al.*, 2008; *Bale et al.*, 2008]. As on Wind, the S/WAVES TDS preferentially selects large amplitude waveform captures for telemetry. S/WAVES also records the peak detector voltage (TDSmax) at a 1 minute cadence, effectively tracking maximum wave activity irrespective of burst waveform telemetry. During the 12 December 2006 perigee passes, the S/WAVES TDS was configured to sample three-component AC electric fields at 31.25 kS/s for an event duration of 524 ms.

[7] The SAMPEX satellite was launched into near polar low earth orbit in July 1992. The 95 minute orbit provides nearly full coverage of magnetic local time and L value over roughly 3 months, or half of its 6 month precession period [*Baker et al.*, 1993]. SAMPEX carries an array of particle detectors designed to measure energetic magnetospheric particle precipitation, as well as galactic and solar cosmic ray energy and composition. The Heavy Ion Large Telescope (HILT) instrument used in this study employs a large geometric factor (roughly 100 cm^2 sr for $\simeq$1 MeV electrons) array of silicon solid state detectors (SSDs) with a 68 × 68° acceptance angle sensitive to electrons with energies ≥1.05 MeV [*Klecker et al.*, 1993; *Blake et al.*, 1996].

3. Observations

[8] On 12 December 2006, the STEREO-B TDS recorded 24 electric field waveforms ranging in amplitude from 100 mV/m to over 240 mV/m [*Cattell et al.*, 2008]. The right-hand circularly polarized waves occurred in bursty packets of duration 0.01 to 0.1 s and exhibited peak power at roughly 0.2 f_{ce}, where f_{ce} is the local electron cyclotron frequency. The TDS waveform captures showing large amplitude waves were sampled from 11:20 to 11:24 UT at $L \simeq 4.7$ at 0330 MLT and −13° magnetic latitude (MLAT). The TDSmax records show that large amplitude waves persisted from 11:05 to 11:25 UT spanning L = 4.2 to 4.8 from 0310 to 0340 MLT with a short gap at 11:15 UT at L = 4.4 at 0320 MLT. Unlike typical lower-band VLF chorus (<0.5 f_{ce}), these obliquely propagating waves did not exhibit the usual dispersive tones typically associated with whistler chorus as described by *Sazhin and Hayakawa* [1992, and references therein].

[9] On 13 November 1998, Wind passed through the nightside radiation belts and captured 17 large amplitude wave events over the course of ten minutes at $L \simeq 4$ at 0200 MLT and 9° MLAT. Peak-to-peak wave amplitudes ranged from 100 mV/m to more than 300 mV/m, with peak wave power at 0.1–0.2 f_{ce}. Again, on 10 April 2000, Wind recorded 28 large amplitude whistler wave packets at $L \simeq 5$ from midnight to 0300 MLT, from 7° to −5° MLAT. These waves exhibited peak-to-peak amplitudes from 100 mV/m to over 400 mV/m with peak power at 0.2–0.3 f_{ce}. The sampled E_x and E_y channels are in the spacecraft spin plane and provide a measurement that roughly corresponds to the x-y GSE electric field. Wave polarization cannot be precisely determined with only the E_x and E_y channels; however, all events exhibit circular polarization in the x-y plane. The polarization for a subset of the observed large amplitude whistler waves has been determined using the three-component wave magnetic field measurements of the WAVES TDSS sampler; the waves were found to range from nearly field-aligned to highly oblique, with wave propagation direction independent of magnetic latitude. All waveforms exhibit the same bursty structure as those reported by *Cattell et al.* [2008], *Cully et al.* [2008], and Kellogg et al. (submitted manuscript, 2010).

[10] Figure 1 shows the SAMPEX HILT count rate per 20 msec for twenty minutes surrounding the times of microburst precipitation for the 13 November 1998 (Figure 1a) and 10 April 2000 (Figure 1b) Wind perigee passes. The SAMPEX satellite is operating in a three-axis stabilized configuration during both intervals, with the HILT detector viewing the local bounce loss cone (BLC); observed microbursts are indicative of relativistic electrons precipitating within their bounce period. During the interval shown in Figure 1a, Wind was located at $L \simeq 4$ at 0200 MLT. SAMPEX recorded powerful microburst precipitation at $L \simeq$ 3–4 from 0330 to 0400 MLT. Wind and SAMPEX were separated by roughly 1.5 hours in local time during the most intense microbursts. On 10 April 2000 at roughly 03:20 UT, microbursts can again be seen in the SAMPEX data at L = 5–6 from 0400 to 0430 MLT (Figure 1b). This precipitation was observed during a two hour interval in which Wind recorded large amplitude whistler waves at $L \simeq 5$ from midnight to 0300 MLT. During the most intense microburst precipitation, Wind and SAMPEX were at roughly the same L shell but separated by four hours in MLT.

[11] Sample Wind TDS burst captures recorded during the precipitation events are included below Figures 1a and 1b. These captures are typical of the bursty, large amplitude whistler-mode waves observed during the passes. The abrupt enhancements in energetic particle flux occur on the same ~0.1 s timescales as the bursty whistler wave packets, consistent with the typical subsecond temporal structure of

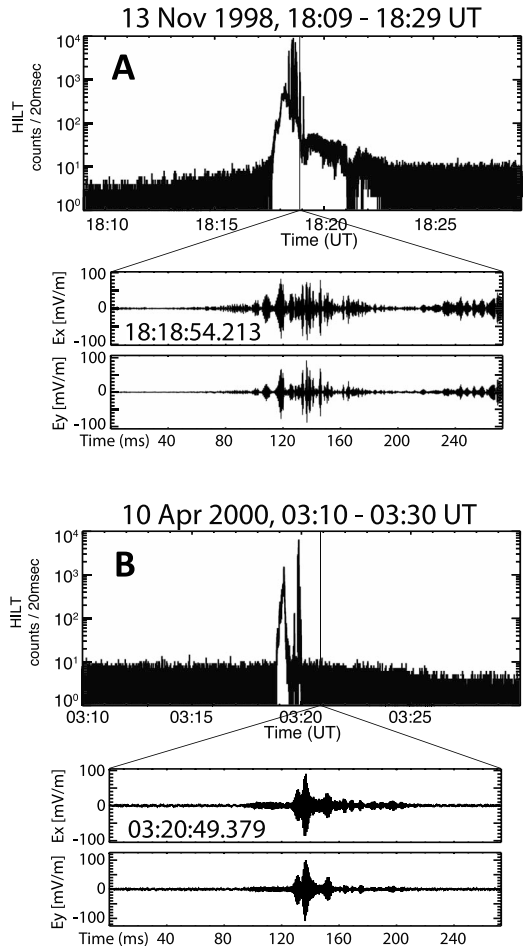

Figure 1. Twenty minutes of SAMPEX HILT counts/20 msec during the (a) Nov 1998 and (b) 10 Apr 2000 events. The counts are summed over the four rows (16 SSDs) of the HILT detector (state 4). TDS captures from are shown below Figures 1a and 1b and are representative of the typical subsecond structure of the large amplitude whistler wave packets.

microburst precipitation [e.g., *Blake et al.*, 1996]; however, due to the lack of peak detector data and the irregularity of the TDS burst captures, it is not possible to determine whether the large amplitude waves occurred in precise conjunction with the observed microbursts. The November 1998 and April 2000 events immediately follow energetic electron injection as indicated by Los Alamos National Laboratory (LANL) energetic electron data, consistent both with the usually invoked free energy source and with *Nakamura et al.*'s [2000] statistical study showing abrupt increases in microburst precipitation following substorm main phase. The AE index exceeds 500 nT during the April 2000 event and approaches 1500 nT preceding the November 1998 event.

[12] The December 2006 STEREO perigee passes provide a unique assessment of radiation belt response to substorm onset, with STEREO-A leading STEREO-B by 1.4 hours (roughly one SAMPEX orbit). This orbital configuration effectively served to bracket a small substorm injection event at 10:50 UT with AE approaching 800 nT [*Cattell et al.*, 2008]. STEREO-A recorded no large amplitude waves during a period of geomagnetic quiet (AE $\simeq$ 100 nT), as evidenced by the STEREO-A TDSmax record plotted in Figure 2a (bottom). The HILT data plotted in Figure 2a (top) shows no microburst precipitation during the same interval, with SAMPEX in near conjunction with STEREO-A.

[13] STEREO-B traversed the same region shortly after the injection event, and TDSmax data reveals persistent large amplitude waves throughout the interval (Figure 2b, bottom). At roughly 11:12 UT located at $L \simeq 4.3$ at 0319 MLT, STEREO-B TDSmax indicates the occurrence of waves with

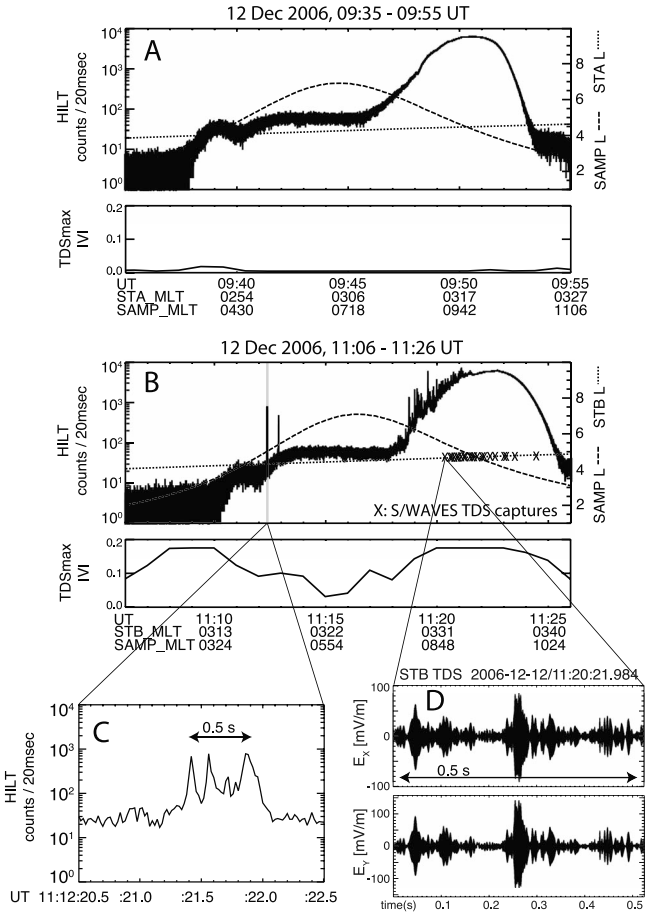

Figure 2. Twenty minutes of HILT counts/20 msec from consecutive SAMPEX orbits coinciding with the STEREO-A and STEREO-B perigee passes. No microburst precipitation is observed in the HILT data during the STEREO-A perigee pass (a), roughly 1.5 hours ahead of the STEREO-B pass (b). The L-shell of the satellites was calculated based on the IGRF-10 magnetic field model and is superposed on the plot of the HILT counts. Their locations in MLT are labeled with the times of the observations. Times of TDS burst captures are marked by ×s along the STEREO-B L-shell trajectory. The peak detector voltage recorded by the STEREO-A/B TDS instrument during each pass is also shown to illustrate the onset of strong wave activity after the STEREO-A pass and the continuous occurrence of large amplitude waves during the observed microburst precipitation. The similarity in the temporal structure of the (c) microburst precipitation and (d) large amplitude whistler wave packets suggests a correspondence between the two phenomena.

peak-to-peak amplitudes approaching 200 mV/m. No TDS burst captures were telemetered at 11:12 UT, but spectral analysis shows peak power at a fraction of the local electron cyclotron frequency, consistent with the whistler mode [*Cattell et al.*, 2008]. At the same time, SAMPEX records powerful microburst precipitation at $L \simeq 4.8$ at 0430 MLT (Figure 2b). The bursty, subsecond structure of the microburst precipitation can be seen in Figure 2c. Strong microburst precipitation is again observed as SAMPEX makes a second pass through $L = 5$–6, this time at 0810–0930 MLT, consistent with *Dietrich et al.*'s [2010] observations of microburst storms extending up to 6 hours in MLT. TDS burst captures recorded at the same time but separated by more than 5 hours in MLT exhibit the typical subsecond wave packet structure (times of occurrence marked with ×s along the STEREO-B L-shell trajectory in Figure 2b, with an example waveform shown in Figure 2d).

[14] The HILT detector was inclined with respect to the background magnetic field during both passes, viewing a combination of BLC and drift loss cone (DLC) particles. The increased background count rate due to the presence DLC particles can be seen in both passes and is attributed to a persistent scattering process occurring eastward of SAMPEX. Due to the isotropy of REMB [e.g., *Blake et al.*, 1996], the bursty flux enhancements can be attributed to relativistic electrons precipitating within the bounce period. The absence of both large amplitude waves and microbursts before substorm injection suggests a connection in the onset of large amplitude whistler wave packets and relativistic electron precipitation in response to substorm activity. This connection is further illustrated by the similarity in the temporal structure and duty cycle of the microbursts and whistler wave packets shown in Figure 2 and discussed by *Cattell et al.* [2008].

4. Discussion

[15] The observations presented herein are drawn from the only known intervals in which a satellite equipped with instruments capable of recording high time resolution, large amplitude waveforms reached near conjunction with a low-altitude satellite capable of measuring relativistic electron precipitation; until data are available from RBSP and BARREL, this represents the best data set with which to examine the possible relationship between large amplitude whistler mode waves and relativistic electron precipitation. These observations provide evidence suggesting a causal connection between large amplitude whistler-mode wave packets and relativistic electron precipitation. The relatively common occurrence of coherent, oblique whistler mode waves with amplitudes exceeding 200 mV/m in the nightside through dawn radiation belts [*Cattell et al.*, 2008; Kellogg et al., submitted manuscript, 2010] suggests a reexamination of whistler wave–particle interactions is necessary for the understanding of radiation belt dynamics. The first-order cyclotron resonance interaction capable of scattering of MeV radiation belt electrons can only occur at high latitudes for the observed wave frequencies; however, higher harmonics of the cyclotron resonance may occur at low latitudes, especially for obliquely propagating whistler-mode waves [*Lorentzen et al.*, 2001; *Millan and Thorne*, 2007, and references therein]. The work of *Meredith et al.* [2001] shows that lower band chorus occurs primarily at low latitudes in the nightside radiation belts, only moving to higher latitudes beginning near dawn and continuing to the dayside. The observation of equatorial large amplitude oblique whistler waves in conjunction with relativistic electron precipitation near midnight suggests that the low latitude interaction with oblique whistler waves may drive the precipitation of MeV electrons.

[16] Much recent work has focused on the detailed simulation and analysis of nonlinear whistler wave–particle interaction. *Omura et al.* [2007] reported that electrons with energies of a few hundred keV may undergo a relativistic turning acceleration during their bounce motion in a dipole field, resulting in acceleration to MeV energies in a single trapping interaction. *Cattell et al.* [2008] described results of simulations showing the rapid acceleration and scattering of energetic electrons due to nonlinear oblique large amplitude whistler wave–particle interactions. Shortly after, *Bortnik et al.* [2008] presented detailed simulations showing that the phase trapping interaction dominates for oblique large amplitude waves. *Tao and Bortnik* [2010] further show that the equatorial region is favored for the nonlinear interaction of non-dispersive, oblique, large amplitude whistler-mode waves with relativistic radiation belt electrons. *Kellogg et al.* [2010] show that the electrostatic component of the oblique large amplitude whistler packets observed by Wind and STEREO is indeed capable of significant electron trapping through resonant interaction, in part consistent with simulations.

[17] These recent simulation studies, coupled with the observed occurrence of strong microburst precipitation in conjunction with coherent, large amplitude whistler waves, indicate that the nonlinear trapping interaction plays an important role in the dynamics of energetic radiation belt electrons. The possible connection between large amplitude whistler waves and relativistic electron precipitation calls for a closer examination of the nonlinear interactions that govern transient electron radiation belt substorm response.

[18] **Acknowledgments.** This work was supported by NASA STEREO grants NNX09AG82G and NNX07AF23G, and by NASA grant NAS5-01072 under contract from APL for the development of RBSP/EFW. Simulation work was carried out using resources of the University of Minnesota Supercomputing Institute with the assistance of Shuxia Zhang. Geosynchronous electron data provided by LANL. DST and AE indices courtesy of WDC for Geomagnetism, Kyoto.

[19] The Editor thanks two anonymous reviewers for their assistance in evaluating this paper.

References

Baker, D. N., G. M. Mason, O. Figueroa, G. Colon, J. G. Watzin, and R. M. Aleman (1993), An overview of the Solar, Anomalous, and Magnetospheric Particle Explorer (SAMPEX) mission, *IEEE Trans. Geosci. Remote Sens.*, *31*, 531–541.

Bale, S. D., et al. (2008), The electric antennas for the STEREO/WAVES experiment, *Space Sci. Rev.*, *136*, 529–547, doi:10.1007/s11214-007-9251-x.

Blake, J. B., M. D. Looper, D. N. Baker, R. Nakamura, B. Klecker, and D. Hovestadt (1996), New high temporal and spatial resolution measurements by SAMPEX of the precipitation of relativistic electrons, *Adv. Space Res.*, *18*, 171–186.

Bortnik, J., R. M. Thorne, and U. S. Inan (2008), Nonlinear interaction of energetic electrons with large amplitude chorus, *Geophys. Res. Lett.*, *35*, L21102, doi:10.1029/2008GL035500.

Bougeret, J. L., et al. (1995), Waves: The radio and plasma wave investigation on the Wind spacecraft, *Space Sci. Rev.*, *71*, 231–263.

Bougeret, J.-L., et al. (2008), S/WAVES: The radio and plasma wave investigation on the STEREO mission, *Space Sci Rev*, *136*, 487–528, doi:10.1007/s11214-007-9298-8.

Burtis, W. J., and R. A. Helliwell (1976), Magnetospheric chorus—Occurrence patterns and normalized frequency, *Planet. Space Sci.*, *24*, 1007–1024.

Cattell, C., et al. (2008), Discovery of very large amplitude whistler-mode waves in Earth's radiation belts, *Geophys. Res. Lett.*, *35*, L01105, doi:10.1029/2007GL032009.

Cully, C. M., J. W. Bonnell, and R. E. Ergun (2008), THEMIS observations of long-lived regions of large-amplitude whistler waves in the inner magnetosphere, *Geophys. Res. Lett.*, *35*, L17S16, doi:10.1029/2008GL033643.

Dietrich, S., C. J. Rodger, M. A. Clilverd, J. Bortnik, and T. Raita (2010), Relativistic microburst storm characteristics: Combined satellite and ground-based observations, *J. Geophys. Res.*, *115*, A12240, doi:10.1029/2010JA015777.

Driesman, A., S. Hynes, and G. Cancro (2008), The STEREO observatory, *Space Sci Rev*, *136*, 17–44, doi:10.1007/s11214-007-9286-z.

Imhof, W., H. Voss, J. Mobilia, D. Datlowe, E. Gaines, J. McGlennon, and U. Inan (1992), Relativistic electron microbursts, *J. Geophys. Res.*, *97*, 13,829–13,837.

Kellogg, P. J., C. A. Cattell, K. Goetz, S. J. Monson, and L. B. Wilson III (2010), Electron trapping and charge transport by large amplitude whistlers, *Geophys. Res. Lett.*, *37*, L20106, doi:10.1029/2010GL044845.

Klecker, B., et al. (1993), HILT: A heavy ion large area proportional counter telescope for solar and anomalous cosmic rays, *IEEE Trans. Geosci. Remote Sens.*, *31*, 542–548, doi:10.1109/36.225520.

Lorentzen, K. R., J. B. Blake, U. S. Inan, and J. Bortnik (2001), Observations of relativistic electron microbursts in association with VLF chorus, *J. Geophys. Res.*, *106*, 6017–6027, doi:10.1029/2000JA003018.

Meredith, N. P., R. B. Horne, and R. R. Anderson (2001), Substorm dependence of chorus amplitudes: Implications for the acceleration of electrons to relativistic energies, *J. Geophys. Res.*, *106*, 13,165–13,178, doi:10.1029/2000JA900156.

Millan, R., and R. Thorne (2007), Review of radiation belt relativistic electron losses, *J. Atmos. Sol. Terr. Phys.*, *69*, 362–377, doi:10.1016/j.jastp.2006.06.019.

Nakamura, R., M. Isowa, Y. Kamide, D. N. Baker, J. B. Blake, and M. Looper (2000), SAMPEX observations of precipitation bursts in the outer radiation belt, *J. Geophys. Res.*, *105*, 15,875–15,885, doi:10.1029/2000JA900018.

Oliven, M. N., and D. A. Gurnett (1968), Microburst phenomena: 3. An association between microbursts and VLF chorus, *J. Geophys. Res.*, *73*, 2355–2362.

Oliven, M. N., D. Venkatesan, and K. G. McCracken (1968), Microburst phenomena: 2. Auroral-zone electrons, *J. Geophys. Res.*, *73*, 2345–2353.

Omura, Y., N. Furuya, and D. Summers (2007), Relativistic turning acceleration of resonant electrons by coherent whistler mode waves in a dipole magnetic field, *J. Geophys. Res.*, *112*, A06236, doi:10.1029/2006JA012243.

Santolík, O., D. A. Gurnett, J. S. Pickett, M. Parrot, and N. Cornilleau-Wehrlin (2003), Spatio-temporal structure of storm-time chorus, *J. Geophys. Res.*, *108*(A7), 1278, doi:10.1029/2002JA009791.

Sazhin, S. S., and M. Hayakawa (1992), Magnetospheric chorus emissions: A review, *Planet. Space Sci.*, *40*, 681–697, doi:10.1016/0032-0633(92)90009-D.

Tao, X., and J. Bortnik (2010), Nonlinear interactions between relativistic radiation belt electrons and oblique whistler mode waves, *Nonlinear Processes Geophys.*, *17*, 599–604, doi:10.5194/npg-17-599-2010.

J. B. Blake and M. D. Looper, Space Science Department, The Aerospace Corporation, 2350 El Segundo Blvd., El Segundo, CA 90245, USA.

A. Breneman, C. A. Cattell, K. Goetz, P. J. Kellogg, K. Kersten, and J. R. Wygant, School of Physics and Astronomy, University of Minnesota, Twin Cities, Minneapolis, MN 55455, USA. (kkersten@physics.umn.edu)

I. Roth, Space Sciences Laboratory, University of California, Berkeley, CA 94720, USA.

L. B. Wilson III, NASA Goddard Space Flight Center, Code 672, Bldg. 21, Room 143A, Greenbelt, MD 20771, USA.